Quantum Chemical Studies of Reactions of the Cyclic Disulfides with the Zinc Finger Domains in the HIV-1 Nucleocapsid Protein (NCp7)

Igor A. Topol,* Alexander V. Nemukhin,† Ming Chao, Lakshmanan K. Iyer, Gregory J. Tawa, and Stanley K. Burt

Contribution from the Advanced Biomedical Computing Center, SAIC Frederick, NCI Frederick Cancer Research and Development Center, P.O. Box B, Frederick, Maryland 21702-1201, and Chemistry Department, Moscow State University, Moscow 119899, Russian Federation

Received February 17, 2000. Revised Manuscript Received May 23, 2000

Abstract: By using quantum chemistry methods, including ab initio Hartree−Fock (HF), as well as the Density Functional Theory approach employing B3LYP approximation, the reaction profiles of three cyclic disulfide species with model zinc finger domains in the HIV-1 nucleocapsid protein (NCp7) have been analyzed. It is shown that the disulfide molecules can act as efficient agents destroying the tetrahedral coordination sphere of the zinc finger domains. The consequence of the reaction is a break of one of the Zn−S bonds and removal of the corresponding molecular thiolate group from the domain by forming a new S−S bond between sulfur atoms from the withdrawing fragment and of the electrophilic agent. As a result of this process the zinc-containing site transforms from the initial tetrahedral geometry to a planar geometry configuration. This transformation further facilitates destruction of the metal binding site. The calculations explicitly show correlations between redox potentials of the electrophilic agents, their reactivity, and barrier heights on the reaction pathway.

I. Introduction

Zinc finger proteins constitute a major group of transcription factors, and play important roles in gene expression at the terminus of cellular signal transduction. The HIV-1 nucleocapsid protein (NCp7) contains two copies of the highly conserved Cys-X2-Cys-X4-His-X4-Cys (CCHC) retroviral zinc finger motif.[1] Each of the two zinc finger domains coordinates one zinc stoichiometrically with three cysteine thiols and a histidine imidazole group and folds into a stable structure.[2] The conservation of the CCHC zinc finger sequences, their resistance to mutations, and their critical roles in multiple phases of the HIV-1 replication cycle make the zinc finger domains attractive targets for the development of antiviral drugs.

The functions of the zinc finger domains are critically dependent on the binding of zinc and the folded conformations stabilized by this zinc binding.[3] Various electrophilic reagents have been identified that cause HIV-1 inhibition by modification of the nucleophilic zinc finger thiolates. Certain oxidizing agents can eject zinc from the fingers and render the virus uninfectious.[4,5] In particular, a variety of disulfide compounds including aliphatic and aromatic, heterocyclic, thiuram and xanthic disulfides have been shown to cause release of zinc from the proteins.[6−11] It was suggested that the reaction mechanism involves an electrophilic attack on a zinc-coordinated cysteine sulfur atom by a sulfur atom of the electrophile, followed by zinc ejection with subsequent intramolecular disulfide bond formation and rearrangement.[12,13]

The extreme importance of such reactions and an absence of direct proofs of the proposed reaction mechanism stimulated our molecular modeling studies. Recent progress in computational ab initio quantum chemistry now allows one to carry out the simulations at the appropriate level of theory. Semiempirical quantum chemistry approaches usually do not provide enough reliability for such complicated molecular systems. Previously, the structures of metal binding sites in zinc finger domains have been modeled by using density functional theory (DFT) methods.[14] Geometric and electronic properties of the metal binding sites belonging to three distinct zinc finger families have been analyzed, and important conclusions about the structure of the domain have been formulated. Deerfield and Pedersen have performed ab initio calculations at the Hartree−Fock/3-

* Address correspondence to this author at the NCI Frederick Cancer Research and Development Center.

† Moscow State University.

(1) Berg, J. M.; Shi, Y. *Science* **1996**, *271*, 1081.

(2) Summers, M. F.; Henderson, L. E.; Chance, M. R.; Bess, J. W., Jr.; South, T. L.; Blake, P. R.; Sagi, I.; Perez-Alvarado, G.; Sowder, R. C.; Hare, D. R.; Arthur, L. O. *Protein Sci.* **1992**, *1*, 563.

(3) Gorelick, R. J.; Nigida, S. M.; Bess, J. W., Jr.; Arthur, L. O.; Henderson, L. E.; Rein, A. J. *J. Virol.* **1990**, *64*, 3207.

(4) Yu, X.; Hathout, Y.; Fenselau, C.; Sowder, R. C.; Henderson, L. E.; Rice, W. G.; Mendeleyev, J.; Kun, E. *Chem. Res. Toxicol.* **1995**, *8*, 585.

(5) Chertova, E. N.; Kane, B. P.; McGrath, C.; Johnson, D. G.; Sowder, R. C.; Arthur, L. O.; Henderson, L. E. *Biochemistry* **1998**, *37*, 17890.

(6) Rice, W. G.; Turpin, J. A.; Schaeffer, C. A.; Graham, L.; Clanton, D.; Buckheit, R. W., Jr; Zaharevitz, D.; Summers, M. F.; Wallquist, A.; Covell, D. G. *J. Med. Chem.* **1996**, *39*, 3606.

(7) Rice, W. G.; Turpin, J. A.; Arthur, L. O.; Henderson, L. E. *Int. Antiviral News* **1995**, *3*, 87.

(8) Fujita, M.; Otsuka, M.; Sugiura, Y. *J. Med. Chem.* **1996**, *39*, 503.

(9) Rice, W. G.; Schaeffer, C. A.; Harten, B.; Villinger, F.; South, T. L.; Summers, M. F.; Henderson, L. E.; Bess, J. W., Jr.; Arthur, L. O.; McDougal, J. S.; Orloff, S. L.; Mendeleyev, J.; Kun, E. *Nature* **1993**, *361*, 473.

(10) Rice, W. G.; Supko, J. C.; Malspeis, L.; Buckheit, R. W., Jr; Clanton, D.; Bu, M.; Graham, L.; Schaeffer, C. A.; Turpin, J. A.; Domagala, J.; Gogliotti, R.; Bader, J. P.; Halliday, S. M.; Coren, L.; Sowder, R. C.; Arthur, L. O.; Henderson, L. E. *Science* **1995**, *270*, 1194.

(11) Tummino, P. J.; Scholten, J.; Harvey, P.; Holler, T. P.; Maloney, L.; Gogliotti, R.; Domagala, J. M.; Hupe, D. *Proc. Natl. Acad. Sci. U.S.A.* **1996**, *93*, 969.

(12) Loo, J. A.; Holler, T. P.; Sanchez, J.; Gogliotti, R.; Maloney, L.; Reily, M. D. J. *J. Med. Chem.* **1996**, *39*, 4313.

(13) Rice, W. G.; Baker, D. C.; Schaeffer, C. A.; Graham, L.; Bu, M.; Terpenong, S.; Clanton, D.; Schultz, R.; Bader, J. P.; Buckheit, R. W., Jr; Field, L.; Singh, P. K.; Turpin, J. A. *Antimicrob. Chemother. Fch* **1997**, *41*, 419.

(14) Topol, I. A.; Casas-Finet, J. R.; Gussio, R.; Burt, S. K.; Erickson, J. W. *J. Mol. Struct. (THEOCHEM)* **1998**, *423*, 13.

10.1021/ja000585x CCC: $19.00
Published on Web 07/08/2000

21G* level, examining the structure and relative acidity for a model Zn(II)-$(H_2S)_2$(imidazole)$_2$ zinc finger site.[15] A semiquantitative analysis of the reactivity of zinc finger domains toward various electrophiles based on DFT calculations is described in the work of Maynard et al.[16] To the best of our knowledge, these works exhaust the list of papers devoted to quantum chemistry calculations on model retroviral zinc fingers.

In this work we describe the first attempt to simulate with quantum chemistry tools the early stage of the reaction of the zinc site with disulfide electrophilic agents, which are considered as potential inhibitors of HIV-1 replication.[13] According to the conclusions drawn from experiments, the sulfur atoms of the zinc coordinating Cys residues (most likely, Cys49) are susceptible to electrophilic attack by certain functional groups.[5,7,13,17] The detailed mechanism of the reactions which finally lead to the ejection of Zn(II) ions is not completely understood. However, it is believed that there is some correlation between the electrophilic agent redox potential (RP) and its reactivity toward ejection of zinc from the NCp7 protein. Reliable values of RP can be computed by using an approach that combines quantum chemistry and dielectric continuum models in the theory of solvation phenomena and, in fact, the results of calculations for a series of disulfide agents perfectly agree with the experimental findings.[18] In this work, we deepen the theoretical analysis and, in addition to calculations of RP, also compute the energy profiles of elementary chemical reactions using quantum chemistry methods. Our primary motivation was to directly relate the redox potentials of the electrophilic reagents and activation barriers on a reaction path for the drug−metal binding site complexes. If such a correlation is firmly established, it promises important applications for efficient searches of potential drugs.

A proper ab initio treatment of the thiolate−disulfide reactions is a complicated task. Bachrach and Mulhearn have shown that the energy profiles for the simple exchange reactions of the type $HS^- + HS{-}HS \rightarrow HS{-}SH + HS^-$ (as well as with a partial substitution of hydrogen by CH_3) have a complicated relief depending on the calculation level.[19,20] In particular, the HF/6-31+G(d) and MP2/6-31+G(d) potential energy surfaces differ in the region of the transition state, and the barrier heights in the entrance channel are substantially lower at the correlated level (for example, 6.3 vs 10.2 kcal/mol). Therefore, for quantitative conclusions post-HF approximations are important; however, given the size of the systems being modeled in this work, this level of calculation is computationally prohibitive. For qualitative purposes and especially for ranking different reagents, the Hartree−Fock level of approximation with proper basis sets provides enough accuracy. To obtain quantitative estimations of the energetic characteristics such as activation barriers and RP values, we employed DFT methods to include electron correlation.

The calculations in this work have been performed with the Gaussian98[21] program by using ab initio Hartree−Fock (HF) and the DFT approach with B3LYP approximation as incorporated in the Gaussian98 package. For the majority of calculations, we used a good quality basis set composed of the conventional 6-31+G(d,p) basis sets on N, O, and S atoms, 6-31G(p) basis set on H atoms, and the recently published 6-31G(f) basis set on Zn.[22] We report the results for equilibrium geometry configurations of reagents and products, reaction path profiles, transition state structures, and RP values of the electrophilic agents. These results are further supported by conclusions drawn using Bader's Atoms in Molecules (AIM) analysis[23] and Weinhold's Natural Bond Orbital (NBO) analysis.[24]

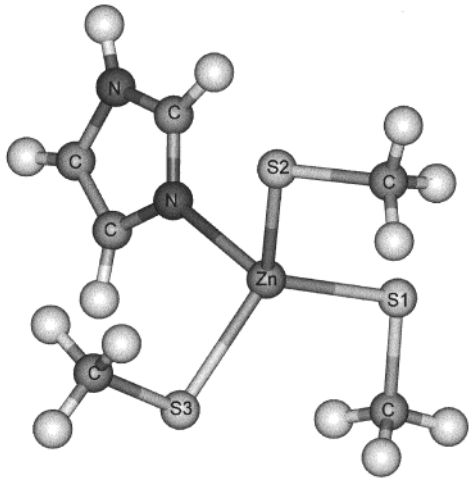

Figure 1. Equilibrium geometry configuration of the model zinc-containing site $[(N_2C_3H_4)Zn(SCH_3)_3]^-$.

II. Computational Strategy and Results

(a) Molecular Models. Previously, it has been shown that the binding of Zn(II) to ligands in the zinc finger domains in NCp7 is determined mainly by interactions with its closest neighbors.[14] This conclusion was taken into account in this work when constructing a simplified model for the CCHC domains. We also took into account that under physiological conditions all three sulfur centers originating from cysteines are deprotonated and bear negative charges. Therefore, the zinc finger site is modeled here by a chelation sphere formed by three methyl thiolates $(SCH_3)^-$ and the imidasole ring around the Zn(II) ion.[14] The coordinates of the HIV-1 nucleocapsid protein were taken from the Protein Data Bank[25] and used for an initial structural guess for this model compound $[(N_2C_3H_4)Zn(SCH_3)_3]^-$. All calculations, including geometry optimizations, have been performed by using the HF and B3LYP methods.

The equilibrium geometry configuration for the zinc-containing model site optimized at the HF level is shown in Figure 1.

(15) Deerfield, D. W.; Pedersen, L. G. *J. Mol. Struct. (THEOCHEM)* **1997**, *419*, 221.

(16) Maynard, A. T.; Huang, M.; Rice, W. G.; Covell, D. G. *Proc. Natl. Sci. U.S.A.* **1998**, *95*, 11578−11583.

(17) Hathout, Y.; Fabris, D.; Han, M. S.; Sowder, R. C., 2nd; Henderson, L. E.; Fenselau, C. *Drug Metab. Dispos*. **1996**, *24*, 1395.

(18) Topol, I. A.; McGrath, C.; Chertova, E.; Dasenbrock, C.; La Course, W. R.; Eissenstat, M. A.; Burt, S. K.; Henderson, L. E.; Casa-Finet, J. R. *J. Med. Chem.* To be submitted for publication.

(19) Bachrach, S. M.; Mulhearn, D. C. *J. Phys. Chem*. **1996**, *100*, 3535.

(20) Mulhearn, D. C.; Bachrach, S. M. *J. Am.Chem. Soc*. **1996**, *118*, 9415.

(21) Gaussian 98, Revision A.7, Frisch, M. J.; Trucks, G. W.; Schlegel, H. B.; Scuseria, G. E.; Robb, M. A.; Cheeseman, J. R.; Zakrzewski, V. G.; Montgomery, J. A., Jr.; Stratmann, R. E.; Burant, J. C.; Dapprich, S.; Millam, J. M.; Daniels, A. D.; Kudin, K. N.; Strain, M. C.; Farkas, O.; Tomasi, J.; Barone, V.; Cossi, M.; Cammi, R.; Mennucci, B.; Pomelli, C.; Adamo, C.; Clifford, S.; Ochterski, J.; Petersson, G. A.; Ayala, P. Y.; Cui, P. Y.; Morokuma, K.; Malick, D. K.; Rabuck, A. D.; Raghavachari, K.; Foresman, J. B.; Cioslowski, J.; Ortiz, J. V.; Baboul, A. G.; Stefanov, B. B.; Liu, G.; Liashenko, A.; Piskorz, P.; Komaromi, I.; Gomperts, R.; Martin, R. L.; Fox, D. J.; Keith, T.; Al-Laham, M. A.; Peng, C. Y.; Nanayakkara, A.; Gonzalez, C.; Challacombe, M.; Gill, P. M. W.; Johnson, B.; Chen, W.; Wong, M. W.; Andres, J. L.; Gonzalez, C.; Head-Gordon, M.; Replogle, E. S.; Pople, J. A. Gaussian, Inc.: Pittsburgh, PA, 1998.

(22) Rassolov, V. A.; Pople, J. A.; Ratner, M. A.; Windus, T. L. *J. Chem. Phys.* **1998**, *109*, 1223.

(23) Bader, R. F. W. *Atoms in Molecules: A Quantum Theory*; Clarendon Press: Oxford Science Publications: Oxford, 1990.

(24) Reed, A. E.; Curtiss, L. A.; Weinhold, F. *Chem. Rev*. **1988**, *88*, 899.

(25) Lee, B. M.; De Guzman, R. N.; Turner, B. G.; Tjandra, N.; Summers, M. F. *J. Mol. Biol*. **1998**, *279*, 633.

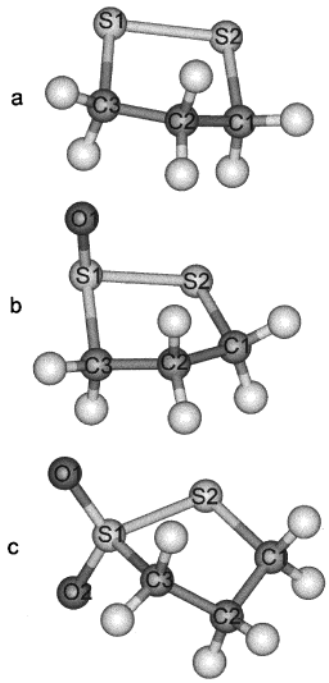

Figure 2. Equilibrium configurations of cyclic disulfide molecules DS (a), DS(O) (b), and $DS(O)_2$ (c).

We note that this structure keeps the main features of the zinc finger domains in NCp7; namely, the characteristic, almost perfect tetrahedral arrangement of the sulfur atoms from cysteine and the nitrogen atom from histidine is clearly seen. In further discussions of transformations of this geometry, we explicitly distinguish one of the thiolate ligands $(SCH_3)^-$, which actively participates in reactions as SCH_3^-, and code the remaining three ligands (imidazole, $N_2C_3H_4$, and two thiolate, SCH_3^-, species) as L_1, L_2, and L_3, respectively Therefore, the molecular model of the zinc finger site is designated here as $(L_1L_2L_3Zn\text{-}SCH_3)^-$.

Figure 2 shows the geometry configurations of three representative molecules, $(CH_2)_3S\text{-}S(A,B)$, of the 1,2-dithiolane class which have been considered as representative electrophilic agents for modeling reactions with the zinc finger domains. For brevity, we denote the simplest cyclic disulfide without oxygen atoms (A and B absent, Figure 2a) as DS, cyclic thiosulfone with one oxygen (A = O, B absent) as DS(O) (Figure 2b), and cyclic thiosulfoxide with two oxygen atoms (A = O, B═O) as $DS(O)_2$ (Figure 2c). The related species of the same class of potential inhibitors of HIV-1 replication have been tested in the experimental studies of ref 13.

The primary goal of this work is to study the mechanism of the reactions

$$(L_1L_2L_3\text{-}Zn\text{-}SCH_3)^- + (CH_2)_3S\text{-}S(A,B) \rightarrow \text{products} \quad (1)$$

by quantum chemistry tools and compare the results for all three A, B combinations, i.e., for DS, DS(O), and $DS(O)_2$. As mentioned in the Introduction, it is firmly established that these potential inhibitors attack the zinc finger domain by breaking one of the Zn−S bonds with the subsequent withdrawal of zinc. We describe below the products and transition states of the first stage of this reaction.

(b) Preliminary Qualitative Considerations. In the initial stages of the modeling, we used the results of the Atoms in Molecules (AIM) and Natural Bond Orbital (NBO) analysis to find the most appropriate reaction coordinate. The AIM theory of Bader[23] deals with the topological properties of the electron density (ρ). If the Laplacian of the charge density $\nabla^2\rho(\mathbf{r})$ is negative, then $\rho(\mathbf{r})$ is greater than its average value at neighboring points and the charge is concentrated in the region around the point $\mathbf{r}$, whereas if $\nabla^2\rho(\mathbf{r}) > 0$, the opposite is true. The minimum in $\nabla^2\rho(\mathbf{r})$ corresponds to the maximum of charge concentration and the maximum in $\nabla^2\rho(\mathbf{r})$ corresponds to the maximum of charge depletion. According to Bader, the sites of electrophilic or nucleophilic attack are related to the sites of maximum charge concentration of charge depletion which are dependent on local maxima or local minima in the Laplacian of charge distribution. Thus, the favorable orientation of the reactants at the early stage of an electrophilic or nucleophilic attack reaction is the alignment of regions of local charge concentrations with regions of local charge depletion.

Table 1. The Properties of Bonds at the Zinc Binding Site and in the Disulfide Molecules Obtained as the Results of the AIM Analysis[a]

bond type	electron density at BCP, au (6.748 e Å^{-3})	Laplacian of electron density at BCP, au (24.1 e Å^{-5})
Zn−S	0.049	0.113
Zn−N	0.063	0.313
C−S	0.134	−0.103
H−C	0.267	−0.850
H−N	0.342	−1.614
C−C	0.324	−0.900
N−C	0.302	−0.602
S−S in DS	0.120	−0.030
S−S in DS(O)	0.096	0.029
S−S in $DS(O)_2$	0.103	0.011

[a] We show typical characteristics of electron density at bond critical points (BCP) which may differ slightly for the same pair of atoms, e.g., for different Zn−S bonds at the zinc binding site. Corresponding structures are shown in Figures 1 and 2.

The topology of $\rho(\mathbf{r})$ or $\nabla^2\rho(\mathbf{r})$ can be analyzed by locating critical points (CP's) in $\rho(\mathbf{r})$ or $\nabla^2\rho(\mathbf{r})$. The CP's, at which $\Delta\rho(\mathbf{r}) = 0$ or $\Delta\nabla^2\rho(\mathbf{r}) = 0$, are represented as (r,s), where the rank r of the CP is equal to the number of nonzero eigenvalues of the Hessian matrix of $\rho(\mathbf{r})$ or $\nabla^2\rho(\mathbf{r})$, and the signature s is the algebraic sum of the signs of the Hessian eigenvalues. In this work, we are mainly interested in the (3,−1) CP for $\rho(\mathbf{r})$ and (3,−3) CP for $\nabla^2\rho(\mathbf{r})$. At the (3,−1) CP in $\rho(\mathbf{r})$, commonly known as bond critical point (BCP), the value of electron density is a minimum along the direction of the bond and a maximum for directions orthogonal to the bond line.

In the NBO analysis[24] the electron density is partitioned in a manner consistent with the Lewis concept of molecular electronic structure theory. The picture of bonding, nonbonding and lone-pair orbitals appears as a result of routine calculations. Numerically estimated composition of an occupied bonding orbital correlates well with the polarity of the corresponding chemical bond. Computed natural charges on atoms provide valuable information about electron density, which are, in most cases, consistent with the AIM data.

Both types of qualitative analysis help to understand binding properties in the molecules, to recognize attacking points, and to select a reaction coordinate for the reagents considered in this paper.

Table 1 summarizes the AIM conclusions concerning the bond properties for all types of chemical bonds occurring in the zinc binding site model shown in Figure 1. Presented are the electron densities and the values of Laplacian of electron density at the BCP's. It should be pointed out that all such parameters are not strongly dependent on the basis sets, therefore, in these calculations a less elaborate basis set has been used compared to the basis sets used for energy estimates. It is clear from the data of Table 1 that the properties of Zn−S bonds

are the most ionic ones demonstrating interaction between closed shell ions. The electron density at the BCP is very low (0.05 au) and has a large positive curvature along the direction of the bond path, which results in the value of $\nabla^2\rho(\mathbf{r})$ being positive at the BCP. This indicates that the charge density is depleted in the interatomic surface between Zn and S. The charge density concentration of the Zn−S bond is not shared but primarily located near the S atom as the maximum bonded charge concentration, a (3,−3) CP in $\nabla^2\rho(\mathbf{r})$, is located only 0.8 Å away from the nucleus of S atom. Though shorter in length, the characteristics of the Zn−N bond are similar to those of the Zn−S bond with a small value of the electron density (0.06 au) and a more positive Laplacian at the BCP, indicating that electron charge concentration is more depleted between Zn and N. Thus, one would expect that the Zn−N bond is more ionic than the Zn−S bond.

Exactly the same conclusions came from the NBO analysis. The NBO procedure unambiguously assigns the Zn−N to the ionic-type bond, while the Zn−S bonds may be equally viewed either as ionic bonds with three lone pairs of electrons on S or as highly polarized toward sulfur covalent bonds.

Interesting conclusions arise from the AIM analysis of disulfide agent molecules. Table 1 also gives the characteristics of bonds in the reagents. Clearly the S−S bonds in these molecules are the weakest of all covalent bond types (beyond S−O). However, a fairly unexpected conclusion is that according to the AIM analysis the tiosulfone compound (S−S(O) bond) might be even more reactive than the thiolsulfoxide one (S−$S(O_2)$ bond).

According to the conclusions of the AIM and NBO analyses, we understand that an attack of the electrophillic agent should be directed on the weakest bond in the zinc-finger domain, namely, on one of the Zn−S bonds. The reaction coordinate may be selected as the distance between two sulfur atoms: one from the incoming agent, one from the zinc-containing site. We expect that the S−S bond in the cyclic disulfide molecules will be broken as a result of the reaction and a new S−S bond appears.

(c) Redox Potentials. The electrophilic compounds DS, DS(O), and $DS(O)_2$ are considered as oxidizing agents that act on zinc finger domains through a redox process; therefore, a comparison of the redox potentials (RP) assigned to each of them provides important information about their relative reactivity. By definition, the reduction of molecule A in solution can be represented by the following equation:

$$A_s + e^- \rightarrow A^-_s \qquad (2)$$

The free energy of this reaction [$\Delta G_s(A \rightarrow A^-)$] corresponds to the absolute redox energy for the above process. The free energy of an electron (e^-) at rest in the gas phase is set to zero.[26] Then, it is possible to calculate the redox energy of reaction 1 using the thermodynamic cycle presented below. In this cycle, ΔG_s-

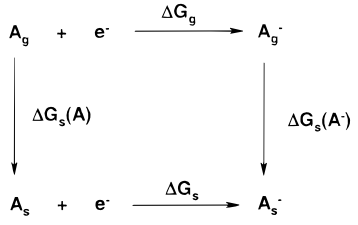

(A) and $\Delta G_s(A^-)$ are the solvation energies of molecule A and its anion A^- (respectively), and $\Delta G_g(A \rightarrow A^-)$ is the free energy difference between molecule A and its anion (which is defined as the redox energy in the gas phase). On the basis of this thermodynamic cycle, one can obtain $\Delta G_s(A \rightarrow A^-)$, the absolute redox energy, as

$$\Delta G_s(A \rightarrow A^-) = \Delta G_g(A \rightarrow A^-) + \Delta G_s(A) - \Delta G_s(A^-) \qquad (3)$$

Thus, by calculating the gas-phase energies and solvation energies of molecule A and its anion A^-, one can derive the absolute redox potential of molecule A in solution. This absolute redox potential can be compared to the experimentally determined one by subtraction of the absolute potential of the hydrogen electrode.

The calculations for all disulfide molecules and their anions considered in this work including thermodynamic parameters in the gas phase were performed using the density functional theory (DFT) method in the B3LYP approximation[27,28] with 6-311++G(d,p) basis sets as implemented in the Gaussian98[21] program packages. The methods of solvation energy calculations used in this work were described in detail in our previous publications.[29,30] Here we just briefly mention the main points of this computational protocol.

The solvation calculations to obtain $\Delta G_s(A)$ and $\Delta G_s(A^-)$ are performed using the B3LYP approximation and a self-consistent reaction field (SCRF) cycle.[31,32] In the SCRF cycle B3LYP calculations are performed on the solutes to obtain an initial electronic energy and charge density in the gas phase. An electrostatic potential fit (ESP[33]) is performed to represent the solute charge density as a set of atom-centered charges. The solvent response to the solute charge distribution is obtained by solving an integral form of the Poisson equation ($\epsilon_{out} = 78.5$, $\epsilon_{in} = 1$) using boundary element methods.[34−45] The reaction field of the solvent is obtained as a set of polarization charges placed on the solute molecular surface. The solute Hamiltonian is then augmented with a Coulomb operator representing the interaction of the polarization charges with the electrons and nuclei of the solute. The calculations are repeated until the electronic energy of the solutes becomes constant. The electrostatic component of the solvation free energy is then given

(26) Zhang, L. Y.; Friesner, R. A. *J. Phys. Chem.* **1995**, *99*, 16479.
(27) Becke, A. D. *J. Chem. Phys.* **1993**, *98*, 5648.
(28) Lee, C.; Yang, W.; Parr, R. G. *Phys. Rev. B* **1988**, *37*, 785.
(29) Topol, I. A.; Tawa G. J.; Burt S. K.; Rashin A. A. *J. Phys. Chem. A* **1997**, *101*, 10075.
(30) Tawa, G. J.; Topol, I. A.; Burt, S. K.; Caldwell, R. A.; Rashin, A. A. *J. Chem. Phys.* **1998**, *109*, 4852.
(31) Tawa, G. J.; Martin, R. L.; Pratt, L. R.; Russo, T. V. *J. Phys. Chem.* **1996**, *100*, 1515.
(32) Rashin, A. A.; Bukatin, M. A.; Andzelm J.; Hagler, A. T. *Biophys. Chem.* **1994**, 51, 375.
(33) Besler, B. H.; Merz, K. M, Jr.; Kollman, P. A. *J. Comput. Chem.* **1990**, 11, 431.
(34) Rashin, A. A.; Young, L.; Topol, I. A. *A. Biophys. Chem.* **1994**, 51, 359.
(35) Rashin , A. A.; Namboodiri, K. *J. Phys. Chem.* **1987**, 91, 6003.
(36) Tawa, G. J.; Pratt, L. R. *J. Am. Chem. Soc.* **1995**, 117, 1625.
(37) Rashin, A. A. *J. Phys. Chem.* **1990**, 94, 1725.
(38) Zauhar, R. J.; Morgan, R. S. *J. Comput. Chem.* **1988**, 9 171.
(39) Yoon B.; Lenhoff, A. M. *J. Comput. Chem.* **1990**, 11 1080.
(40) Corcelli, S. A.; Kress, J. D.; Pratt, L. R.; Tawa, G. J. *Pacific Symosium on Biocomputing '96*; World Scientific: River Edge, NJ, 1995; p 143.
(41) Mohan, V.; Davis, M. E.; McCammon, J. A.; Pettitt, B. M. *J. Phys. Chem.* **1992**, 96, 6428.
(42) Simonson, T.; Brunger, A. T. *J. Phys. Chem.* **1994**, 98, 4863.
(43) Bharadway, R.; Windemuth, A.; Sridharan, S.; Honig, B.; Nicholls, A. *J. Comput. Chem.* **1995**, 16, 898.
(44) Pratt, L. R.; Tawa, G. J.; Hummer, G.; Garcia, A. E.; Corcelli, S. A. *Int. J. Quantum Chem.* **1997**, 64, 121.

Table 2. Redox Potentials (RP) and the Corresponding Energy Contributions (See Eq 2) Computed for the Disulfide Agents at the B3LYP/6-311++G(d,p) Level

energies	DS	DS(O)	$DS(O)_2$
neutral molecule (A), au	−914.396034	−989.606405	−1064.828545
anionic molecule (A^-), au	−914.428916	−989.654471	−1064.889462
$\Delta G_g(A \rightarrow A^-)$, kcal/mol	22.74	33.37	41.50
$\Delta G_s(A)$, kcal/mol	−0.77	−7.26	−8.93
$\Delta G_s(A^-)$, kcal/mol	−58.95	−60.77	−62.28
RP, kcal/mol	80.93	86.88	94.85

by[32,46]

$$\Delta G_{el} = E(\rho^s) - E^0(\rho^g) + \frac{1}{2}\int_V V(\mathbf{r},\sigma)\rho^s(\mathbf{r})\, d^3r \qquad (4)$$

where $E^0(\rho^g)$ is the quantum mechanical energy of the unperturbed solute evaluated using its gas-phase orbitals, $E(\rho^s)$ is the quantum mechanical energy of the solute evaluated using its solvated orbitals, and $V(\mathbf{r},\sigma)$ is the electrostatic potential at a point **r** within the solute molecular surface. This is due to the surface polarization charge density, σ. ρ^s is the charge density at position **r** of the perturbed (solvated) solute, and the integral describes the energy lowering due to interaction with the solvent.

The *solvent accessible surfaces*[47] of the solutes, SAS, are then constructed using a water probe radius of 1.4 Å, and the nonpolar radii $R(O) = 1.40$ Å[34,35] (the hydrogen atoms are not explicitly included in the SAS calculation). The nonpolar components of the solvation enthalpy and the entropy change of the solvent due to localized order around the solutes were calculated from the SAS according to the procedures suggested in refs 34 and 35. In all solvation calculations the atomic cavity radii of Rashin et al.[34,35] have been used.

The electrostatic and nonpolar solvation free energy components for each molecule and its anion were used to obtain the full solvation free energies, $\Delta G_s(A)$ and $\Delta G_s(A^-)$, in the B3LYP approximation. These energies and the gas-phase free energy of an electron abstraction ($\Delta G_g(A \rightarrow A^-)$) were used to calculate the absolute RP ($\Delta G_s(A \rightarrow A^-)$) according to eq 3.

We present in Table 2 the results of the B3LYP/6-311++G(d,p) calculations of the RP's. According to these calculations, insertion of oxygen atoms into the electrophilic disulfide molecule should lead to noticeable increase of the RP and therefore to higher reactivity of the compound.

(d) Energy Profiles. The greatest computational efforts have been directed to obtain energy profiles for the reactions of the compound modeling the zinc-finger binding site with electrophilic agents and to locate the transition states. As a reaction coordinate we selected the distance between two sulfur atoms R_{SS}, one from the zinc site and another from the disulfide molecule. While keeping this coordinate fixed during partial geometry optimizations, all other geometry parameters were allowed to adjust the minimum energy requirement for a series of points along R_{SS}. Then the transition state (TS) structures were found, i.e., the configurations with precisely one imaginary vibrational frequency. The differences of energies corresponding to the TS configurations and those of the reagents allowed us to estimate the energy barriers of chemical reactions 1. It should be noted that as the energy of reagents we take the energy of the entire system at the beginning of the entrance channel, i.e., at $R_{SS} = 5.4$ Å and with vanished hydrogen bonds between disulfides and metal binding site, thereby eliminating basis set superposition errors. It should be noted that these calculations using reasonably large basis sets and including geometry optimizations for such all-electron 36−38 atomic systems approach the limit of modern computational facilities.

Qualitatively, the flow of the reaction is visualized as follows. Upon approaching the disulfide molecule at the zinc-site, an elongation of the corresponding Zn−S bond in the site and of the S−S bond in disulfide is clearly seen. At some critical point the $(SCH_3)^-$ group is removed from the metal binding site and joined to the electrophilic agent. In this respect the mechanism is consistent with the findings of refs 19 and 20 for simple trisulfide exchange reactions. The changes in geometry structures are noticeable: while initial equilibrium configuration of the zinc-containing site (Figure 1) shows almost tetrahedral arrangement of the ligands around the metal ion, the configuration of the product corresponds to the planar ZnS_2N construct. We do not focus on discussing the changes in geometry of another reaction partner since the primary focus of our attention is on the zinc finger domain.

The general picture of reaction energy profiles for all three disulfide reagents (DS, DS(O), $DS(O)_2$) shows no dramatic changes of the curves along the reaction coordinate. The energy is gradually increasing when the reactants approach each other in the entrance channel and after reaching the transition state barrier a sharp decrease of energy occurs. At the HF level of calculations, the energy barriers are noticeable: 20.9 kcal/mol for DS, 14.2 kcal/mol for DS(O), and 12.6 kcal/mol for $DS(O)_2$. At the B3LYP level, the shapes of the potential curves are almost barrierless: only for DS can a quantitative estimate of 2.1 kcal/mol be firmly established, while for DS(O) and $DS(O)_2$ the energy curves in the entrance channel are particularly flat showing some weak features in the regions corresponding to the region of the HF transition states. However, the structural changes of the complex along the reaction path R_{SS} have the same features in both HF and B3LYP approximations. To check these B3LYP-induced changes of the reaction profile we performed MP2 calculations of the selected points on the reaction profile at the HF and B3LYP optimized geometries. In both cases we obtained energy profiles which were very close to the reaction curves obtained in the B3LYP approximation: no barriers and steady energy drop for $DS(O)_2$ and DS(O), and a small barrier of ~2.9 kcal/mol for DS. It should be mentioned that these MP2 results have only semiquantitative value. They do not show "real" barrier heights which can be obtained only by complete geometry optimizations at the MP2 level. Unfortunately, at present such calculations for a given basis set and size of the models used in our calculations are extremely computationally demanding.

It is known[47,48] that the DFT approximations can substantially underestimate barrier heights on reaction profiles, while HF theory generally overestimates them. Therefore, we believe that the activation energies for the first stage of reaction 1 lie within the limits (2 ÷ 20) kcal/mol for DS and (0 ÷ 14) kcal/mol for DS(O) and $DS(O)_2$. More importantly, for our purposes, is the tendency of changes of the activation energies within this series of reagents, rather than the precise values of energies themselves. It should be considered as well established that the oxygen-containing disulfide reagents DS(O) and $DS(O)_2$ are characterized by noticeably lower activation energies than the simple cyclic disulfide DS, and the difference between mono- and

(45) Tawa, G. J.; Pratt, L. R. In *Structure and Reactivity in Aqueous Solution: Characterization of Chemical and Biological Systems*; ACS Symp. Series 568; Cramer, C. J., Truhlar, D. G., Eds.; American Chemical Society: Washington, DC, 1994; p 60.

(46) Tomasi, J.; Persico, M. *Chem. Rev.* **1994**, 94, 2027.

(47) Baker, J.; Andzelm, J.; Muir, M.; Taylor, P. R. *Chem. Phys. Lett.* **1995**, *237*, 53.

(48) Porezag, D.; Pedersen, M. R. *J. Chem. Phys.* **1995**, *105*, 9345.

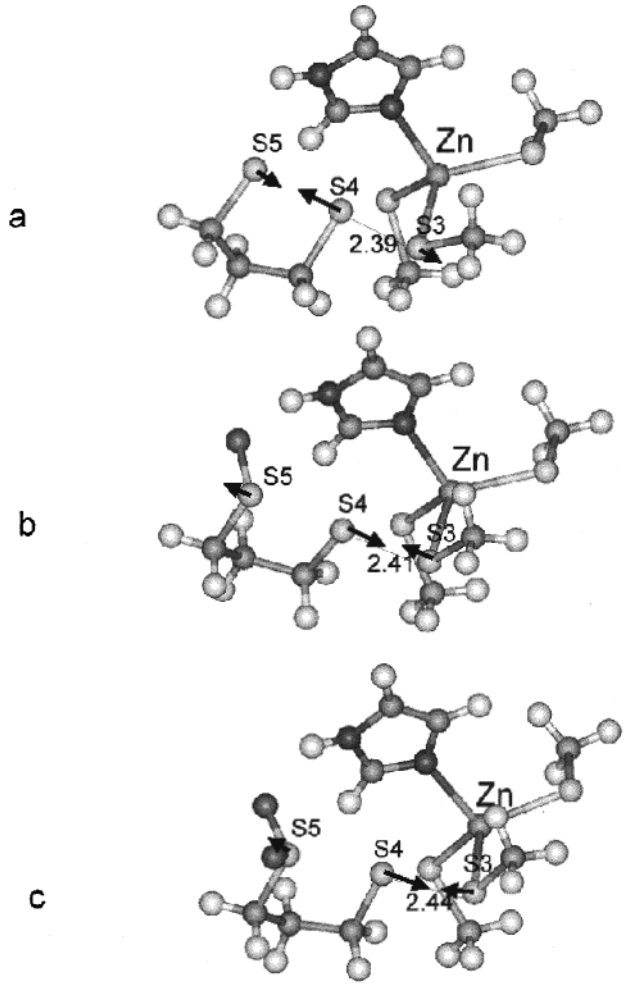

Figure 3. Geometry configurations of the transition states obtained in the Hartree−Fock approximation. Panels a, b, and c correspond to the reagents DS, DS(O), and $DS(O)_2$ respectively. Distance S3−S4 corresponds to the reaction coordinate R_{SS}. Arrows show the main components of the displacement vector for the first vibration (imaginary frequency) at the TS.

dioxygen compounds in this respect is small enough. These conclusions are consistent with the results of the AIM analysis **(**see Table 1) which shows the electronic properties of the S−S bonds that are broken in the course of the reaction.

We display in Figure 3 (panels a−c) geometry configurations of the transition states found at the HF level. It should be noted that in the vicinities of these points on the corresponding potential energy surfaces, sharp changes of geometry configurations occur when reaction coordinate R_{SS} varies only slightly, e.g. within 0.1−0.2 Å. Therefore, a severe reconstruction of the reacting complex in the course of reaction is typical in this case. In particular, the reaction product corresponding to the zinc finger domain ($L_1L_2L_3Zn$) shows a perfect planar geometry configuration around the metal center (Figure 4) in strong contrast to a tetrahedral arrangement in the initial position (Figure 1). It should be mentioned that the $(SCH_3)^-$ anionic group is transferred from the zinc-finger model site to the model drug reagent, and therefore considerable changes in geometry of the reacting species are not unexpected.

Let us analyze the features of the TS's in more detail. As is easy to see from Figure 3, the Zn metal binding site retains tetrahedral coordination at the TS. The geometry changes in the attacking disulfide molecules are determined mainly by S−S bond stretching. Thus, the TS of the reaction could be

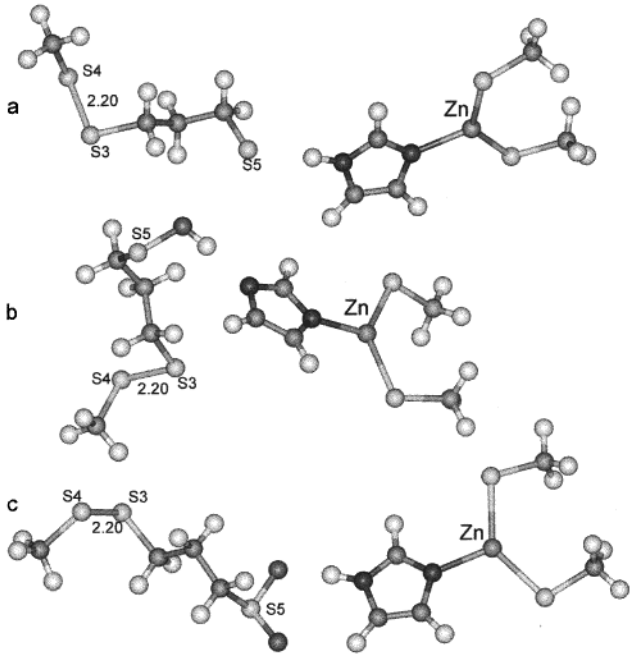

Figure 4. Geometry configuration of the zinc-finger binding site after abstraction of thiolate ligand occurred. Panels a, b, and c correspond to the reagents DS, DS(O), and $DS(O)_2$, respectively. Distance S3−S4 corresponds to the reaction coordinate R_{SS}.

characterized as reagent-like. The first imaginary frequency for all the found TS's has a value around -250 ± 10 cm^{-1}. The normal-mode analysis showed that the main components of the displacement vector for this frequency are oriented along the $S_3-S_4-S_5$ bond (see Figure 3). Besides, the effective mass for this vibration is close to 18. That means that practically only sulfur atoms are involved in this vibration. These considerations obviously justify our choice of the reaction coordinate on one hand and, on the other hand, show that the procedure of moving along the reaction coordinate and locating the TS in the present work is similar to the procedure used in the IRC approach.

Another important reason to analyze geometry configurations of the transition states is to verify whether these configurations match the cavities available in zinc finger domains in the HIV-1 nucleocapsid protein (NCp7). To answer this question, we used the molecular modeling program Insight II[49] to model the docking of the fragment of the most extended transition state corresponding to the $DS(O)_2$ reagent into the real structure of NCp7.[25] We found, first, that there is enough space in the cavity of NCp7 to include the agent and, second, that the choice between two possible attacked sites in NCp7, i.e., finger 1 (Cys15, Cys18, Cys28, His23) or finger 2 (Cys36, Cys39, Cys49, His44), favors the latter option. In the case of finger 2 the distortions (although reasonable in both variants) of the protein structure are less (RMS deviation of the heavy atoms coordinated the Zn atom being 0.5 Å), and therefore this domain (finger 2) should be more attractive for the reagent. Besides, the docking of the TS structure into the metal binding site shows clearly that the best fit can be achieved by attacking Cys49 (Figure 5). Such a conclusion from the theoretical analysis is in agreement with the results of experimental studies, according to which the Cys49 group is the most probable target of the attack.[5]

We also manually docked the product complex into the NCp7 protein on finger 2. We superimposed the product structure onto the original NMR protein structure and in this orientation the

(49) Insight II, Molecular Simulations Inc.: San Diego, 1998.

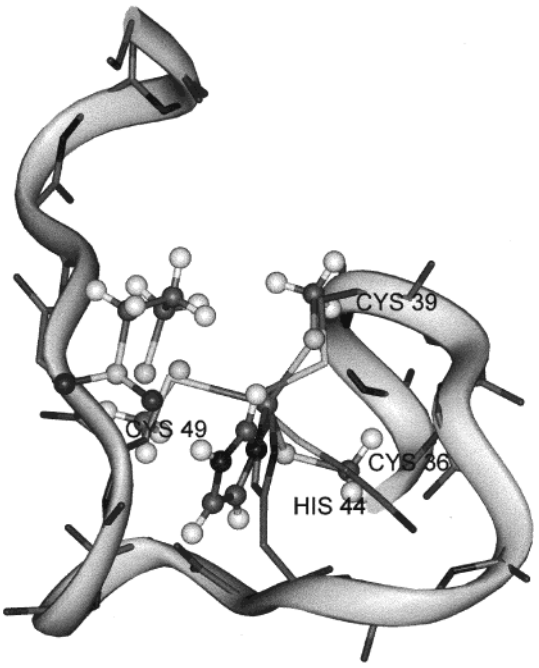

Figure 5. Docking of the TS structure corresponding to the reaction of the reagent $DS(O)_2$ with the metal binding site into the second zinc-finger domain of the NCp7 proteine. Ball and stick fragments correspond to the calculated TS structure. Stick and ribbon fragments correspond to the experimental structure of the second zinc finger region in the NCp7 proteine.[25]

product was oriented completely outside the protein. This means that the stereochemical requirements of the reaction ensure that the product can be released from the finger site with minimal disturbance of the protein backbone structure.

III. Discussion and Conclusions

The Zn-finger CCHC motif is specific for retroviruses and its structural integrity is important for virus replication. Since this particular structural motif is involved in AIDS propagation, understanding its structure and the role that zinc plays in maintaining structural integrity is important for the design of new anti-AIDS therapies. Destruction of the zinc binding sites by immediate attacks of electrophiles, in particular, should have dramatic consequences on the functionality of HIV-1 nucleocapsid protein NCp7. Therefore, we have tried to answer the following questions regarding the NCp7 metal binding site by quantum chemical simulations: What factors are responsible for tetrahedral arrangements of ligands around zinc? How easily can this arrangement be destabilized? How can efficient reagents which disrupt such tetrahedral sites be predicted? What is the result of destabilization of the zinc coordination sphere? How easy is it to remove Zn from the distorted site compared to the initial tetrahedral arrangement?

We believe that the present work assists in answering some of these important questions. We are able to describe in full the initial stage of a chemical reaction, including the reagents, products, and transition states, for the process leading to inhibition of HIV-1 replication:

$$(L_1L_2L_3\text{-Zn-SCH}_3)^- + (CH_2)_3S\text{-S(A,B)} \rightarrow [(L_1L_2L_3\text{-Zn}\cdots CH_3S\cdots S\cdots S(A,B)(CH_2)_3]^- \rightarrow (L_1L_2L_3\text{-Zn}) + (CH_3S\text{-S}\cdots S(A,B)(CH_2)_3)^- \quad (5)$$

We can distinguish the common features of reaction 5 for all three 1,2-dithiolane reagents. A concerted elongation of the Zn−S bonds from the zinc site and S−S bonds from the disulfide molecule is responsible for the energy barrier on the reaction path. An alignment of the reagents in such a way that three sulfur atoms are in almost perfect linear arrangement is required for the configuration of a transition state. After passing the barrier, the system transforms to a configuration in which the zinc site is left in a planar configuration while a detached thiolate ligand joins the disulfide reagent. Therefore, this reaction has some features of the S_N2 mechanism of nucleophilic substitution at sulfur[19,20] in the sense of typical geometry changes during the transformations. For a much simpler model of the thiolate−disulfide exchange reaction, Bachrach and Mulhearn have demonstrated[19,20] that while HF calculations are consistent with the S_N2 mechanism, the methods which include electron correlation effects lead to results more consistent with an addition−elimination mechanism. We cannot exclude that a higher-level treatment of reaction 5 will suggest a more elaborated reaction scheme, but a precise classification of these reactions does not seem an important goal of this study.

Table 3. Properties of the 1,2-Dithiolanes[a]

reagent	RP, kcal/mol	barrier height of reaction 5, kcal/mol	"reactivity" as defined in ref 13
DS	80.93	20.9	0
DS(O)	86.88	14.2	4.9
$DS(O)_2$	94.85	12.6	18

[a] Redox potentials (RP) and barrier heights for reaction 5 are computed in this work. The column "reactivity" is taken from ref 13, and the data show a relative measure of ability of ring-substituted (4,4-di-CH_2O-acetoxy)-1,2-dithiolanes to react with the zinc finger domains of NCp7. More precisely, these values refer to the rate of the increase of concentration of zinc, withdrawn from the protein by a reaction with the oxidizing agents.

Differences among three disulfide agents are due to their ability to attach the negatively charged particles, and a clear correlation between several important parameters is illustrated in Table 3. We see that both theoretical quantities are mutually consistent: the larger the redox potential of the reagent the higher its reactivity toward reaction 5. This is reflected by the lower value of the energy barrier. At the B3LYP level the characteristic of reactivity is an energy change at the points $R_{SS} = 2.5$ and 2.2 Å. This energy change corresponds to energy lowering due to strong structural deformation and was equal to 15.7, 10.2, and 5.5 kcal/mol for $DS(O)_2$, DS(O), and DS molecules, respectively.

Such correlation is important by itself; however, even stronger statements may be formulated if we take into consideration some experimental results. The last column of Table 3 is taken from ref 13, and the data show a relative measure of the ability of ring-substituted (4,4-di-CH_2O-acetoxy)-1,2-dithiolanes to react with the zinc finger domains of the NCp7 protein. The values shown in column 3 of Table 3 are an indication of the relative rate of increase of zinc in the solution due to the interaction of the drug with the zinc finger protein and to the ejection of zinc. Thus, this is a measurement of the relative disruptive power of the compounds. Although a direct comparison of calculated theoretical quantities (redox potential and barrier heights) calculated on molecular models should be viewed with a substantial amount of skepticism, an obvious qualitative correlation between theoretical results and experimental properties is very promising. In a previous study,[18] it has been shown that the rate of reaction of various electrophilic compounds with HIV-1 nucleocapsid protein (experimentally measured) increases in a linear manner with their oxidative power. This correlation was reflected by redox potentials computed by quantum

chemistry methods.[18] In this work the next important step is carried out, namely, we explicitly show that the activation energy of the first stage of the reaction is the rate-limiting parameter. This parameter should be included in the chain of correlations between theoretical and experimental values. From the pragmatic point of view predictions based on redox potentials are much easier to achieve than characterization of the transition state, which demands considerable computational resources. However, characterizing the reaction path allows one to better understand the correlation between redox potentials and reactivity. To investigate specificity it is important to study the reaction pathway.

Beyond consideration of the reaction paths, some qualitative conclusions regarding electrostatic interactions in the studied complexes which can be drawn from the present studies are worth discussing. According to the NBO analysis, zinc in the complex bears the charge close to +1.5 while all four closest atoms (nitrogen from the imidazole ring and three sulfur atoms from the groups which mimic cysteine thiols) bear negative charges slightly less than −1. Mutual repulsion of four substantial negative charges favors almost tetrahedral geometry of the atoms surrounding zinc. It is interesting that the effective electronic configuration of zinc in the model system can be represented as $3d^{10}4s^{0.5}$ assuming some population of the 4s-orbital. This does not assist directionality of the binding, but affects donor−acceptor properties of Zn···S coordinations. It is not easy to classify the Zn−S bonding in the zinc-finger domains. These interactions can be assigned either to chemical bonds with a very high fraction of ionicity ($Zn^{+}\cdots S^{-}$) or to coordination (donor−acceptor) bonds (Zn···S) with some evidence of covalency. This conclusion is mutually supported by both AIM and NBO analyses.

The electrostatics are dominating for the other model complexes considered in this work. The disulfide agents possess considerable electron affinities, and thus high redox potentials. As a consequence they readily extract one of the groups surrounding zinc by breaking one of the Zn−S bonds. In our model studies, the group SCH_3^- migrates to the disulfide species forming a true covalent S−S bond with a new partner, and simultaneously the negative charge is transferred from the zinc-containing complex creating a planar configuration of the remaining ligands. The electronic structure of zinc in the product is essentially the same as in the initial complex, namely, $3d^{10}$-$4s^{0.5}$ with the same effective charge on Zn, +1.5. The amount of negative charge on the three remaining atoms (N, S, S) surrounding zinc is also essentially the same as before the reaction, and pure electrostatics favors planar arrangement of the zinc site.

We believe that removal of zinc from the planar geometry configuration of the site, which is formed after the reaction destroying the tetrahedral domain, is an easy process because of steric factors. It is much easier for a zinc-extracting agent to reach the metal if it is in the planar site than in the tetrahedral one. In addition to the steric factors, energetic factors also play a role. To estimate the energetic contribution we performed calculations which roughly estimate this contribution. Starting from the equilibrium geometry configurations of our model zinc-finger reagent (tetrahedral zinc site) and of the product (planar zinc site) we removed the metal, and computed the energies of the zinc-less sites without changing the geometry of the other atoms. Comparison of summed energies of such structures with that of isolated zinc on one hand and energies of zinc-containing complexes on the other hand shows that more energy is required to withdraw the metal from the tetrahedral site than from the planar site. This energy gain (approximately 10−15% of the binding energy) is of the same scale for removal of either neutral or doubly ionized metal atom.

In summary, we stress that in this work the minimum energy profiles have been computed for three disulfide species, modeling the drugs and interacting with the zinc finger domain of the NCp7 protein. We have specified products of the reaction and transition states. It has been shown that the geometry configurations of transition states are consistent with the spatial restrictions of the second finger domain of NCp7 protein, and a clear correlation between activation energies, redox potentials, and reactivities of the electrophilic agents has been established.

Acknowledgment. We thank the staff and administration of the Advanced Biomedical Computing Center for their support of this project. This project has been funded in whole or in part with Federal funds from the National Cancer Institute, National Institutes of Health, under Contract No. NO1-CO-56000. A.V.N. thanks the Russian Foundation for Basic Researches for partial support (Project No. 98-03-33168). The content of this publication does not necessarily reflect the views or policies of the Department of Health and Human Services, nor does mention of trade names, Commercial products, or organization imply endorsement by the U.S. Government.

Supporting Information Available: An X-ray crystallographic file in CIF format. This material is available free of charge via the Internet at http://pubs.acs.org.

JA000585X